PERGAMON

International Journal of Heat and Mass Transfer 43 (2000) 2869–2882

International Journal of HEAT and MASS TRANSFER

www.elsevier.com/locate/ijhmt

Evaporation heat transfer and pressure drop of R-22 in 7 and 9.52 mm smooth/micro-fin tubes

K. Seo, Y. Kim*

Dept. of Mechanical Engineering, Korea University, Anam-Dong, Sungbuk-Gu, Seoul 136-701, South Korea

Received 4 June 1999; received in revised form 21 October 1999

Abstract

This paper reports heat transfer coefficients and pressure drops during the evaporation of R22 at low evaporating temperatures that corresponds to the operating conditions of a heat pump in the heating mode. Heat transfer measurements were performed for 3.0 m long smooth and micro-fin tubes with the outer diameters of 9.52 and 7.0 mm, respectively. The range of test parameters in the present study includes the evaporating temperature from −15 to 5°C, the refrigerant mass flux from 70 to 211 kg/m^2 s and the heat flux from 5 to 15 kW/m^2. The objective of this study is to evaluate the effectiveness of the micro-fin tube over the smooth tube as a function of the evaporating temperature and tube diameter.

1. Introduction

The micro-fin tube has received increasing attention in recent years due to advantages in view of efficiency and compactness of a heat exchanger over a smooth tube. Generally, it is known that the micro-fin tube, having a larger heat transfer area than the smooth tube, induces annular flow pattern and results in a higher heat transfer coefficient. Schlager et al. [1] reported the evaporation heat transfer coefficient for three tubes with outside diameter of 12.7 mm having different fin height, number of fins and helix angle. The average heat transfer coefficients in the micro-fin tubes were 1.6 to 2.2 times larger for evaporation than those in the smooth tube. The pressure drop increased, but by a smaller factor than the heat transfer coefficient. Evaporating temperatures were varied from 0 to 6°C.

Kuo and Wang [2,3] tested performance of micro-fin tubes with the outside diameters (OD) of 9.52 mm and 7.0 mm using R-22 as a function of mass flux (100–300 kg/m^2 s), heat flux (6–12.4 kW/m^2) and evaporating temperatures (6 and 10°C). It was reported that the evaporation heat transfer coefficients increased with mass flux, heat flux and evaporating temperature. The heat transfer enhancement factor (EF) for the 9.52 mm OD micro-fin tube was approximately 2.2, while for the 7.0 mm OD micro-fin tube, the EF was 1.6. The EF was defined as the ratio of the heat transfer coefficient of a micro-fin tube to that of a comparable smooth tube. The EF considers effect of the increase in surface area of the micro-fin tube.

A heat pump transfers heat from the low-temperature heat source to the high-temperature heat sink. It can be utilized in cooling as well as heating of space by changing the flow direction as to the operational mode. When it operates in the heating mode, the evaporating temperature ranges from −20 to 10°C,

* Corresponding author. Tel.: +82-2-3290-3366; fax: +82-2-921-5439.

E-mail address: yongckim@kuccnx.korea.ac.kr (Y. Kim).

0017-9310/00/$ - see front matter
PII: S0017-9310(99)00338-5

Nomenclature

C	constant in Chisholm correlation
$dP_{F,f}$	frictional pressure drop difference in the liquid phase (N/m^2)
$dP_{F,g}$	frictional pressure drop difference in the vapor phase (N/m^2)
EF	heat transfer enhancement factor
G	mass flux (kg/m^2 s)
h	heat transfer coefficient (W/m^2 K)
i_{fg}	latent heat of vaporization (kJ/kg)
l	test section length (m)
l_x	length of each measurement section (m)
$\dot{m}$	mass flow rate (kg/s)
P	pressure (N/m^2)
PF	pressure drop penalty factor
Q_{in}	average electric power input (W)
q''	heat flux (W/m^2)
T_e	evaporating temperature (K)
T_{in}	inlet temperature of refrigerant (K)
T_{out}	outlet temperature of refrigerant [K]
$T_{w,in}$	average inner wall temperature [K]
T_r	refrigerant temperature [K]
X	Martinelli parameter.
x	vapor quality
Δx	difference of vapor quality

Greek symbol

ϕ_f^2	two-phase friction multiplier for liquid flowing alone

Subscripts

F	friction
f	liquid phase
g	vapor phase
i	local
in	inlet
out	outlet
r	refrigerant
w	wall

which is dependent on the outside temperature. However, most of the previous studies on the evaporation heat transfer inside the tube were focused on evaporating temperatures beyond 0°C with high heat flux conditions. In addition, most of the published data are very limited to the local heat transfer coefficient and heat flux in the practical range. Further study is required for the heat transfer coefficient at lower

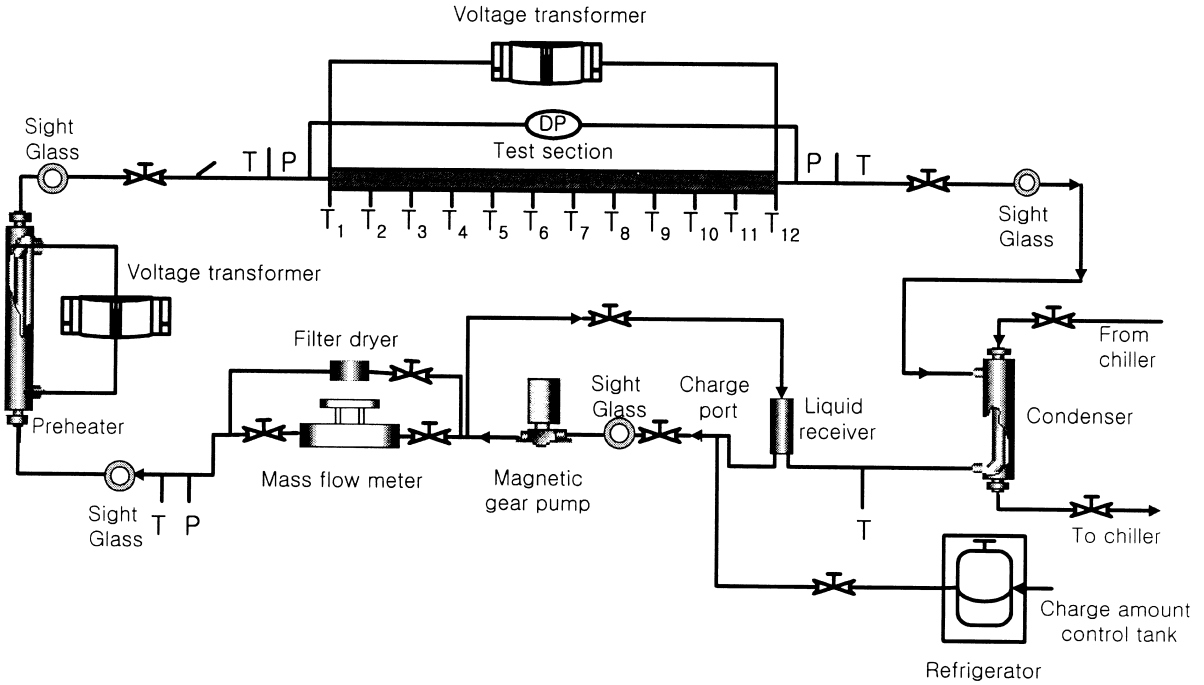

Fig. 1. Schematic diagram of the experimental set-up.

Table 1
Dimension of the tubes tested

Parameter	Test tube			
	smooth		micro-fin	
Outside diameter (mm)	9.52	7.0	9.52	7.0
Average thickness (mm)	0.41	0.41	0.35	0.32
Average inside diameter (mm)	8.70	6.18	8.82	6.36
Maximum inside diameter (mm)	8.70	6.18	8.92	6.46
Fin-height (mm)	–	–	0.12	0.15
Helix angle β (°)	–	–	25	18
Number of fins	–	–	60	60
Inside surface area (cm^2/m)	273.3	194.2	392.7	304.3
Surface area ratio($A_{micro\text{-}fin}/A_{smooth}$)	1.0	1.0	1.44	1.57

evaporating temperature to enhance the performance of heat exchangers applied to heat pumps. Experiments were conducted with a variation of mass flux, heat flux, evaporating temperature and tube diameter to provide extended data on heat transfer and pressure drop of R-22 flowing inside a tube.

2. Experimental apparatus

The test set-up was designed to measure the local heat transfer coefficient and pressure drop of the refrigerant flowing through the test tube. The test loop consisted of liquid pump, preheater, test section and condenser. Fig. 1 shows the schematic of the experimental set-up. Liquid pump with the variable speed motor circulated the subcooled liquid refrigerant to the preheater. Inlet quality of the test section was adjusted by the electric power input supplied to the preheater. Heat flux to the test section was provided using the rope heater with 2 mm diameter. The refrigerant having high quality at the exit of the test section cooled in the condenser and then returned to the liquid pump.

The refrigerant flow rate through the test section was mainly controlled by adjusting the rotational speed of the motor in the pump and partially maintained by regulating the opening of the valves in the main line and the bypass line of flow path from the pump. Due to the wide range of evaporation temperatures (−15 to 5°C) tested in the present study, the amount of refrigerant charge was varied significantly. For easy regulation of refrigerant charge inside the system, the refrigerant vessel was connected to the suction side of the pump. It was kept inside of the refrigerator to extract the refrigerant from the system to the vessel. The charge amount inside the system was adjusted by regulating the needle valve at the inlet of the refrigerant vessel with respect to the evaporating temperature.

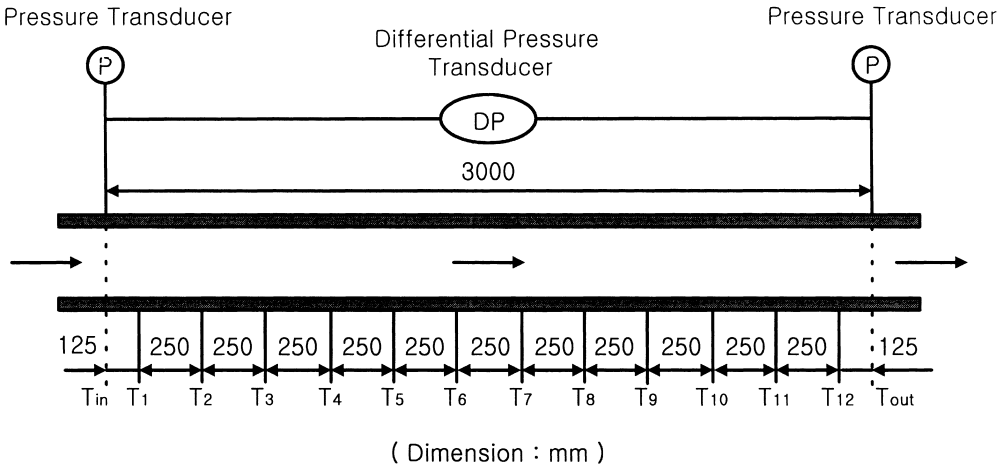

Fig. 2. Schematic diagram of the test section.

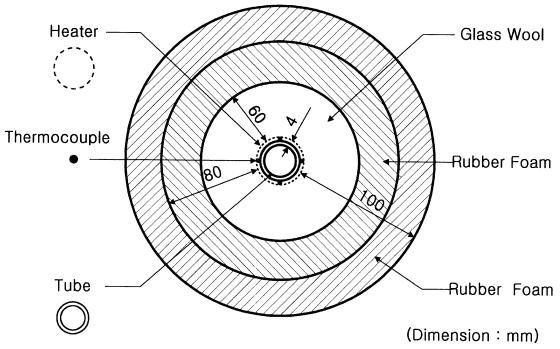

Fig. 3. Cross sectional view of the test section.

A Coriolis effect flowmeter with an uncertainty of ±0.2% reading measured the flow rate of refrigerant entering the test section. The power input to the preheater and the test section was monitored using the power meter with an uncertainty of ±0.1% full scale. All temperatures in the system were measured using the T-type thermocouple with an uncertainty of ±0.1°C. Uncertainty for the thermocouple was estimated at the stand-alone state. The pressure of the refrigerant entering the test section was monitored with the pressure transducer with an uncertainty of ±2.1 kPa, while the pressure drop across the test section is measured with the differential pressure transducer.

Four tubes were tested during this study. The tubes used in the present study were 3.0 m long with an 9.52 and 7.0 mm OD tube. The average inner diameter (ID) of the smooth and micro-fin tube for the 9.52 mm OD was 8.70 and 8.82 mm, respectively, while for the 7.0 mm OD tube it was 6.18 and 6.30 mm, respectively. The 9.52 mm OD micro-fin tube had a 25° spiral angle and fin height of 0.12 mm, while the 7.0 mm OD micro-fin tube had a 18° spiral angle and fin height of 0.15 mm. The area used in the calculation of heat transfer coefficient and mass flux was based on the average inner diameter of the micro-fin tubes. The average inner diameter indicates the equivalent diameter having a wetted cross sectional area for the micro-fin tube. Table 1 shows the dimension of the test tubes.

Surface temperatures in the test section were measured with 48 thermocouples soldered to outside of the tube. The rope heater (2 mm OD) was wrapped around the thermocouple junctions. Location of the thermocouples in the test section is shown in Fig. 2. Measurements were made at 90° intervals around the outer tube circumference at each location. Fig. 3 shows the cross sectional view of the test section. The test section was heavily insulated with glass wool and double layers of rubber foam to reduce heat gain from the surrounding. The residual heat transfer through the ambient was considered in the determination of heat flux using the calibration data.

Table 2
Test conditions for smooth and micro-fin tubes

Mass flux G (kg/m^2 s)	Heat flux q'' (kW/m^2) at evaporating temperature (T_e)		
	−15°C	−5°C	5°C
70	5	5	5
117	5	5	5
164	5	5	5
	10	10	10
	15	15	15
211	5	5	5

3. Experimental conditions and data reduction

Experiments were performed with pure R-22. The evaporating temperature was varied from −15 to 5°C and the refrigerant mass flux from 70 to 211 kg/m^2 s. For the mass flux of 164 kg/m^2 s, the heat flux was varied from 5 to 15 kW/m^2 to investigate the effects on the heat transfer coefficient. Except for the mass flux of 164 kg/m^2 s, the heat flux was fixed at 5 kW/m^2 for the given evaporating temperature. The test conditions are summarized in Table 2.

The local heat transfer coefficient h was defined by Eq. (1).

$$h = \frac{q''}{T_{w,in} - T_r} \tag{1}$$

where q'' is the local heat flux. The average inner wall temperature, $T_{w,in}$, was calculated from the measured

Table 3
Summary of uncertainties of primary and derived parameter

Primary parameter	Uncertainties	Derived parameter	Uncertainties
$\dot{m}$	±0.2 % of reading	G	±1.4%
T	±0.1°C	q''	±1.8%

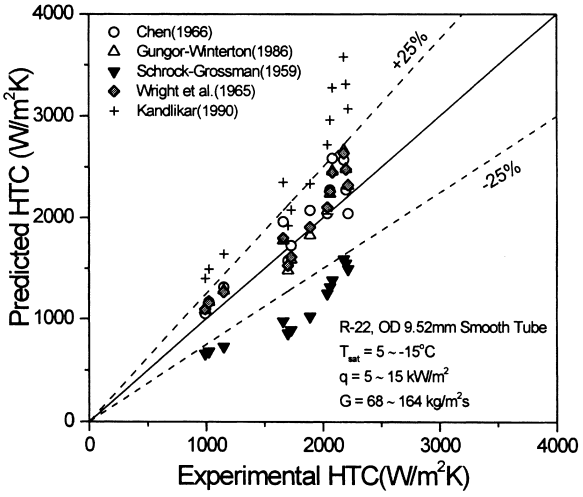

Fig. 4. Comparison of the experimental heat transfer coefficient with the predicted value using heat transfer correlations for the 9.52 mm OD smooth tube.

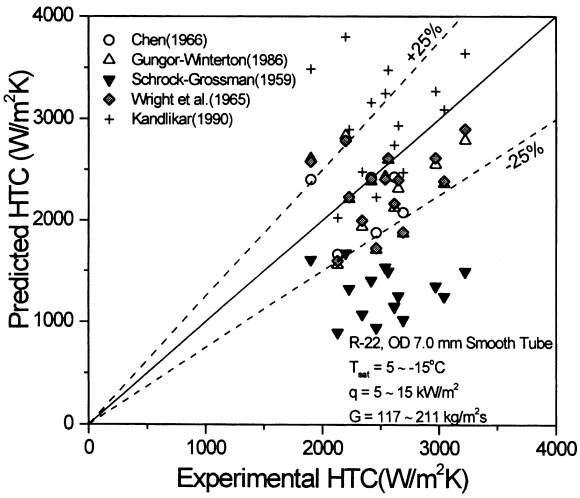

Fig. 5. Comparison of the experimental heat transfer coefficient with the predicted value using heat transfer correlations for the 7.0 mm OD smooth tube.

outside wall temperature using the equation of steady-state radial heat conduction through the tube. Refrigerant temperature T_r inside the tube decreased due to pressure drop through the test section and calculated from the linear interpolation that was defined by Eq. (2).

$$T_r = T_{in} - (T_{in} - T_{out}) \times \frac{l_x}{l} \tag{2}$$

where T_{in} and T_{out} are the inlet and outlet refrigerant temperature of the test section, respectively. The l_x is the length of each measurement section and l is the length of the entire test section.

Local quality x in the test section is estimated by Eq. (3).

$$\Delta x = \frac{Q_{in}}{\dot{m} \times i_{fg}} \tag{3}$$

where $\dot{m}$ is the mass flowrate (kg/s) and Q_{in} is the power input (kJ/s) to the test section.

The difference of the inlet and outlet quality of the test section ($=\Delta x$) was varied with test conditions. For example, when the inlet quality of the test section was 0.1 at the mass flux of 164 kg/m^2 s and heat flux of 5 kW/m^2, the outlet quality of the test section was approximately 0.3. Therefore, to obtain the quality of 0.9 at the outlet of the test section, 4 consecutive experiments (48 local stations) were conducted with different inlet qualities. The average heat transfer coefficients and qualities were calculated by Eq. (4). The local pressure drops were also measured from 4 consecutive experiments with different inlet qualities.

$$\bar{h} = \frac{\sum h_i x_i}{\sum x_i}, \bar{x} = \frac{\sum h_i x_i}{\sum h_i} \tag{4}$$

Uncertainties of the heat transfer coefficients were estimated using a propagation of error analysis [4]. The uncertainties of test parameters and heat transfer coefficients are tabulated in Tables 3 and 4, respectively. The large uncertainties were predicted at a low heat flux due to the small difference in the temperature.

Table 4
Estimated uncertainties of heat transfer coefficient

Heat flux (kW/m^2)		$q'' = 5$		$q'' = 10$		$q'' = 15$	
Outer diameter (mm)		9.52	7.0	9.52	7.0	9.52	7.0
$G = 164$ kg/m^2 s	smooth	±5%	±8%	±3%	±4%	±3%	±3%
	micro-fin	±19%	±11%	±6%	±5%	±4%	±3%

4. Experimental results

The evaporation heat transfer data were taken at the evaporating temperature ranging from 5 to −15°C, the heat flux from 5 to 15 kW/m^2 and the mass flux from 70 to 211 kg/m^{2}s. The experimental data for the heat transfer coefficient and pressure drop were verified by comparing them with the existing empirical models. In the present study, the effects of evaporating temperature, heat flux, tube diameter and mass flux on the heat transfer coefficient in smooth and micro-fin tubes were investigated. The pressure drop was also analyzed as a function of evaporating temperature, mass flux and heat flux.

4.1. Effect of evaporating temperature and heat flux

Figs. 4 and 5 show the average heat transfer coefficients for smooth tubes with 9.52 and 7.0 mm OD, respectively, as compared to the correlations from the literature. For the 9.52 mm OD smooth tube, the Schrock and Grossman [5] correlation under-predicts the experimental data by more than 25%, while the Kandlikar [6] correlation over-estimates the heat transfer data by more than 25%. The predicted values by the correlations of Gungor and Winterton [7], Chen [8] and Wright [9] are consistent with the experimental data and lie within ±25% of the experimental data. This agreement lends confidence to the instrumentation and test methods. For the 9.52 mm OD smooth tube, Kuo and Wang [2,3] recommended the Gungor and Winterton [7] correlation as the closest model to their experimental data.

The predicted heat transfer coefficient for the 7.0 mm OD smooth tube showed a larger deviation from the experimental data than those for the 9.52 mm OD smooth tube because the existing models were generally developed for the larger diameter and higher mass flux conditions. As noted from Fig. 5, the effects of diameter on the heat transfer coefficients were under-estimated as the diameter decreased. Therefore, a correlation considering the effects of diameter should be developed.

The effect of the evaporating temperature and heat flux on the local heat transfer coefficient can be observed from Figs. 6 and 7. Fig. 6 shows variation of local evaporation heat transfer coefficient as a function of quality and evaporating temperature at the mass flux of 164 kg/m^2 s and heat flux of 5 kW/m^2 for the 9.52 mm OD tubes. For the smooth tube, the variation of heat transfer coefficient as a function of quality was very small compared to the micro-fin tube. The evap-

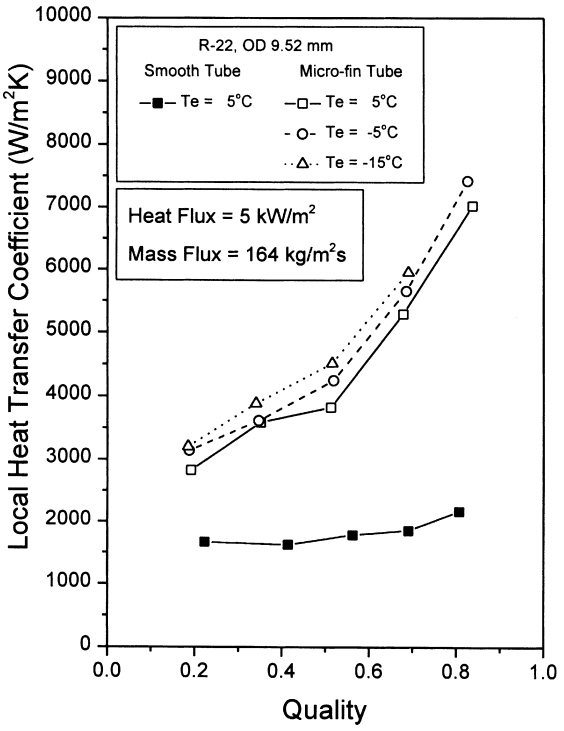

Fig. 6. Local heat transfer coefficients with a mass flux of 164 kg/m^2 s and heat flux of 5 kW/m^2.

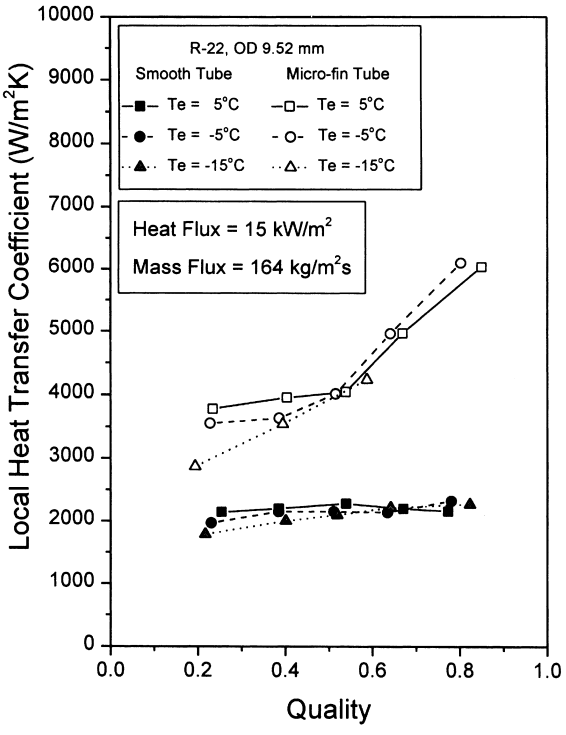

Fig. 7. Local heat transfer coefficients with a mass flux of 164 kg/m^2 s and heat flux of 15 kW/m^2.

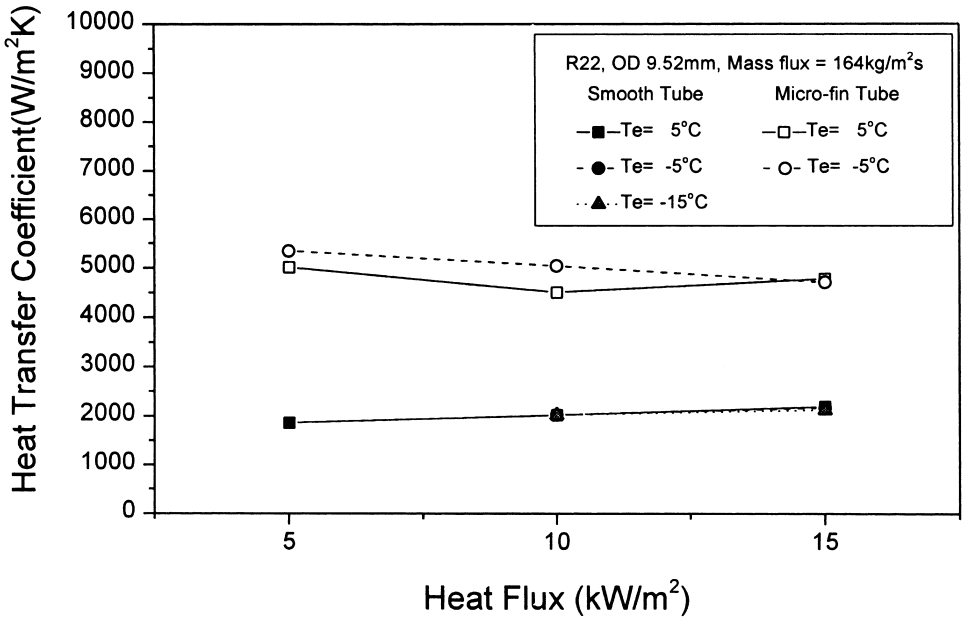

Fig. 8. Average heat transfer coefficients with a mass flux of 164 kg/m^2 s.

oration heat transfer coefficient for the micro-fin tube was approximately 80 to 200% higher than that for the smooth tube. The enhancement of the heat transfer coefficient for the micro-fin tube over the smooth tube increased as the quality was raised. The heat transfer coefficient increased as the evaporating temperature was lowered for the 9.52 mm OD micro-fin tube. Eckels and Pate [10] and Kuo and Wang [2,3] reported that the heat transfer coefficient for the micro-fin tube enhanced as the evaporating temperature increased from 5 to 15°C. However, they did not report any data for the evaporating temperature below 0°C. The

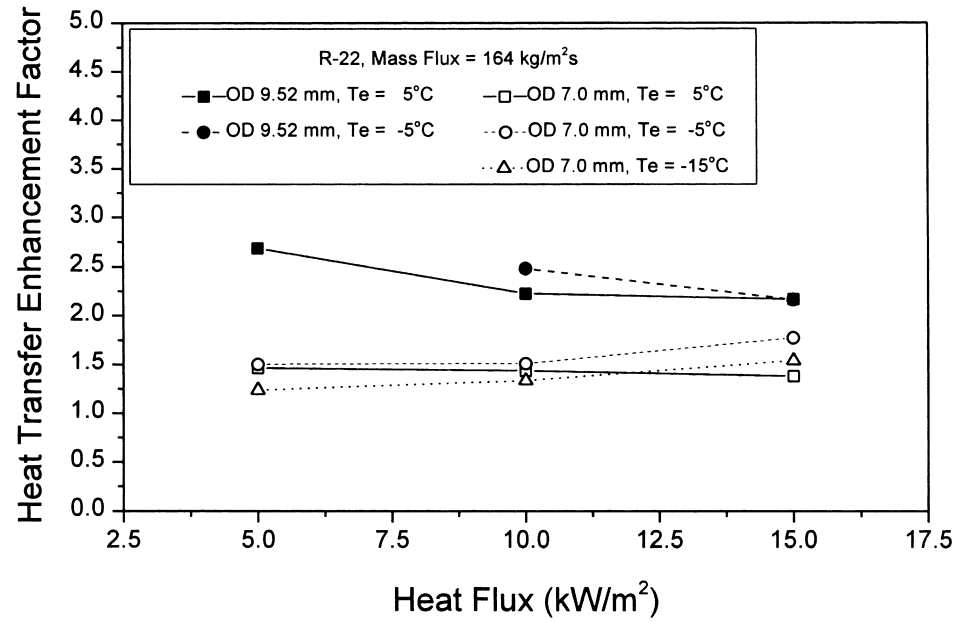

Fig. 9. Heat transfer enhancement factor with a mass flux of 164 kg/m^2 s.

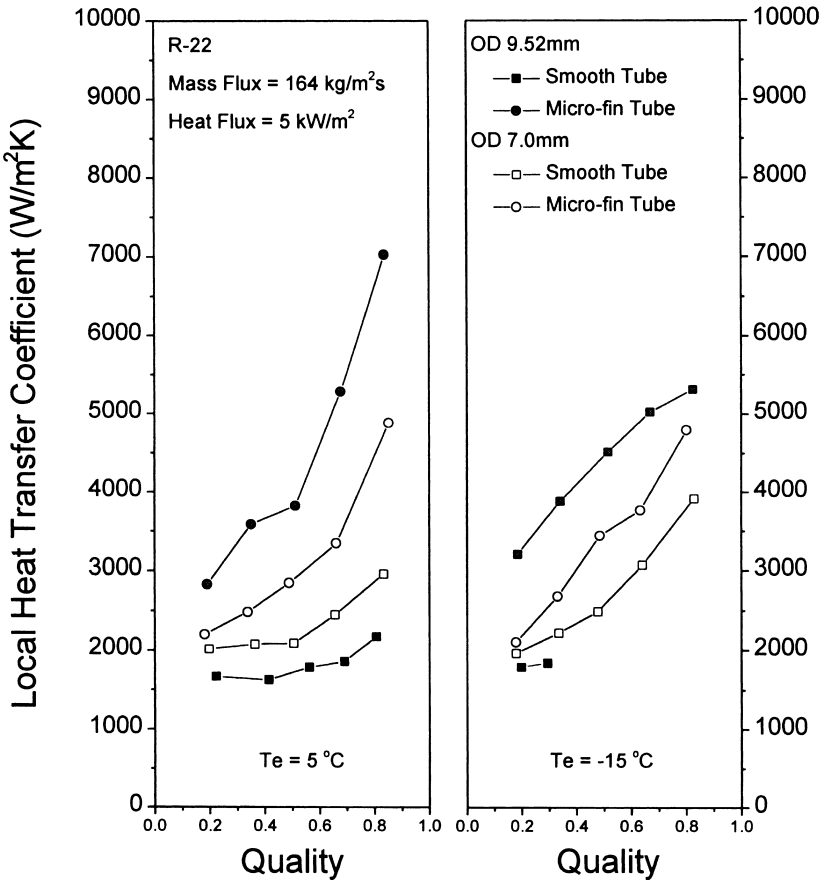

Fig. 10. Local heat transfer coefficients with an evaporating temperature of 5 and −15°C and a heat flux of 5 kW/m^2.

smooth tube shows a relatively small change in the heat transfer coefficient with respect to the evaporating temperature.

Fig. 7 shows the local evaporation heat transfer coefficient at the heat flux of 15 kW/m^2. For the higher heat flux (Fig. 7), the heat transfer coefficient at the low quality region was relatively enhanced as compared to the lower heat flux as shown in Fig. 6. The effect of the heat flux on the heat transfer coefficient was significant at the low quality region, because nucleate boiling was promoted at the low quality region as the heat flux increased. However, for the high quality region the effects of heat flux were very small because the heat transfer at this region was dominated by convective evaporation.

Fig. 8 shows the average heat transfer coefficient vs. heat flux varying the evaporating temperature. For the smooth tube, the evaporation heat transfer coefficient at the heat flux of 15 kW/m^2 was approximately 18% higher than that at the heat flux of 5 kW/m^2. For the micro-fin tube, the evaporation heat transfer coefficient was slightly dropped with the heat flux at the fixed evaporating temperature. Thus, as shown in Fig. 9, the EF for the 9.52 mm OD tube with the evaporating temperature of 5°C drops from 2.7 to 2.2 as the heat flux increases from 5 to 15 kW/m^2. However, the EF values for the 7.0 mm OD tube with the evaporating temperature of 5 and −5°C do not change with the heat flux and it is approximately equal to 1.5. Kuo and Wang [2,3] reported that the EFs of the 9.52 and 7.0 mm OD micro-fin tube with R-22 were approximately 2.2 and 1.6, respectively and the enhanced level was not varied with the heat flux.

4.2. Effect of inner diameter

Fig. 10 shows the variation of the local heat transfer coefficient as a function of quality at a mass flux of 164 kg/m^2 s and heat flux of 5 kW/m^2. The effects of tube diameter on the heat transfer coefficient were drastically changed by varying tube surface from smooth to micro-fin shape. The heat transfer coefficient for the 7.0 mm OD smooth tube was approximately 30% higher than that for the 9.52 mm OD smooth

tube, whereas the heat transfer coefficient for the 9.52 mm OD micro-fin tube was approximately 40% higher than that for the 7.0 mm OD micro-fin tube. Difference of the heat transfer coefficient between the 7.0 mm OD smooth and micro-fin tube was smaller than that between the 9.52 mm OD smooth and micro-fin tube. This would indicate that the micro-fin inside a tube is more effective in the larger tube diameter. Kuo and Wang [2,3] also reported the same trends as the present results. However, Klimenko [11] reported that heat transfer coefficients were not strongly dependent on the tube diameter in convective boiling region. Thus, additional studies are necessary to verify the effects of tube diameter on the heat transfer coefficients.

4.3. Effect of mass flux

Fig. 11 shows variation of the heat transfer coefficient as a function of quality with the 9.52 mm OD tubes at the evaporating temperatures of 5 and −15°C and heat flux of 5 kW/m^2. Generally, the local heat transfer coefficients for both micro-fin and smooth tubes increased with a rise of the mass flux. The enhancement of the heat transfer coefficient with the mass flux was relatively equivalent in all qualities tested in the present study. These results were also observed in most of the previous research [2,3].

Fig. 12 shows the averaged heat transfer coefficient as a function of the mass flux at the heat flux of 5 kW/m^2. Generally the averaged heat transfer coefficient was enhanced as the mass flux increased. The micro-fin tubes showed a slightly higher slope of heat transfer coefficients than the smooth tubes. For the 7.0 mm OD tube, the effects of the evaporating temperature were obvious as compared to those for the 9.52 mm OD tube. The heat transfer coefficient for the 7.0 mm OD tube dropped as the evaporating temperature were varied from −15 to 5°C. The 9.52 mm OD micro-fin

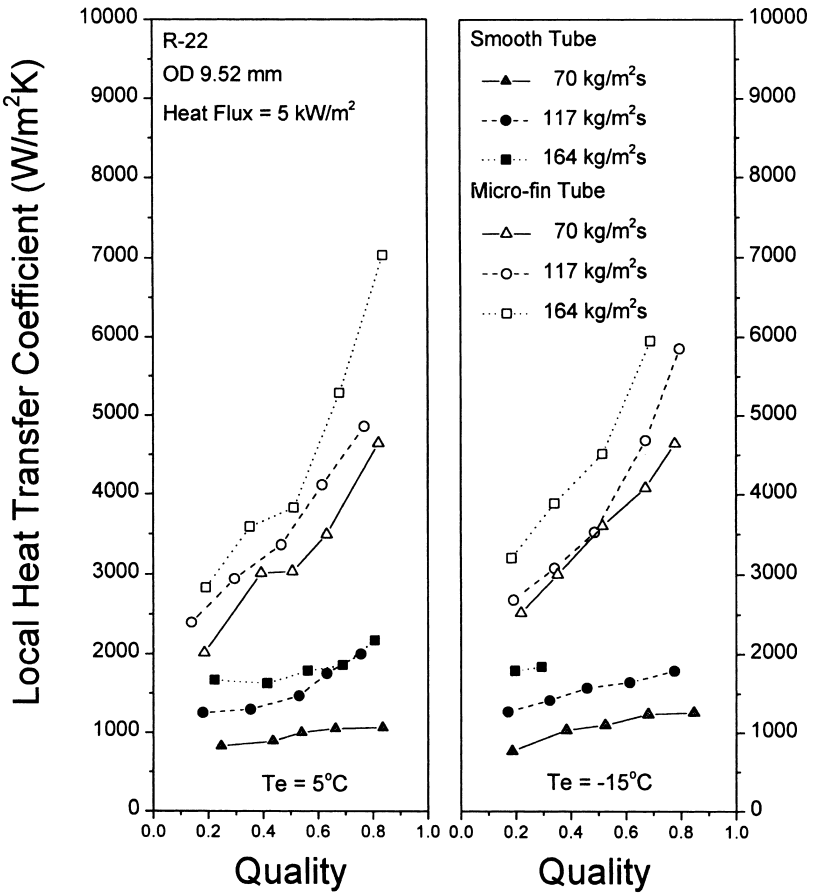

Fig. 11. Local heat transfer coefficients with an evaporating temperature of 5 and 15°C and a heat flux of 5 kW/m^2.

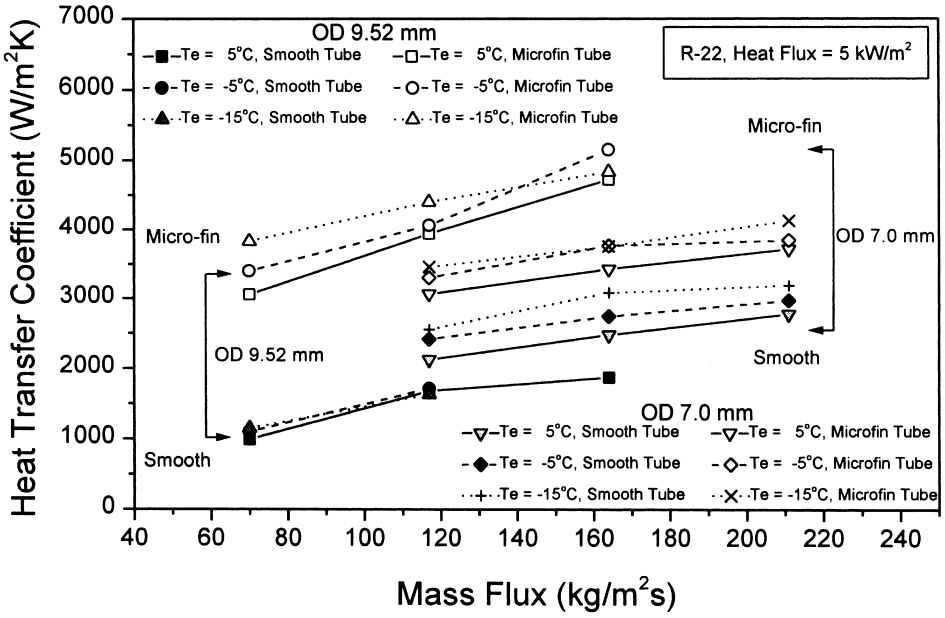

Fig. 12. Average heat transfer coefficients with a heat flux of 5 kW/m^2.

tube showed the highest heat transfer coefficients among the tubes tested.

As shown in Fig. 13, the EFs for the 7.0 mm OD tube ranged from 1.2 to 1.4, while the EFs for the 9.52 mm OD tube varied from 2.4 to 3.3 in all test conditions. For the 9.52 mm OD tube, the EFs reduced as the mass flux increased from 70 to 117 kg/m^2 s and it was slightly raised as the mass flux increased from 117

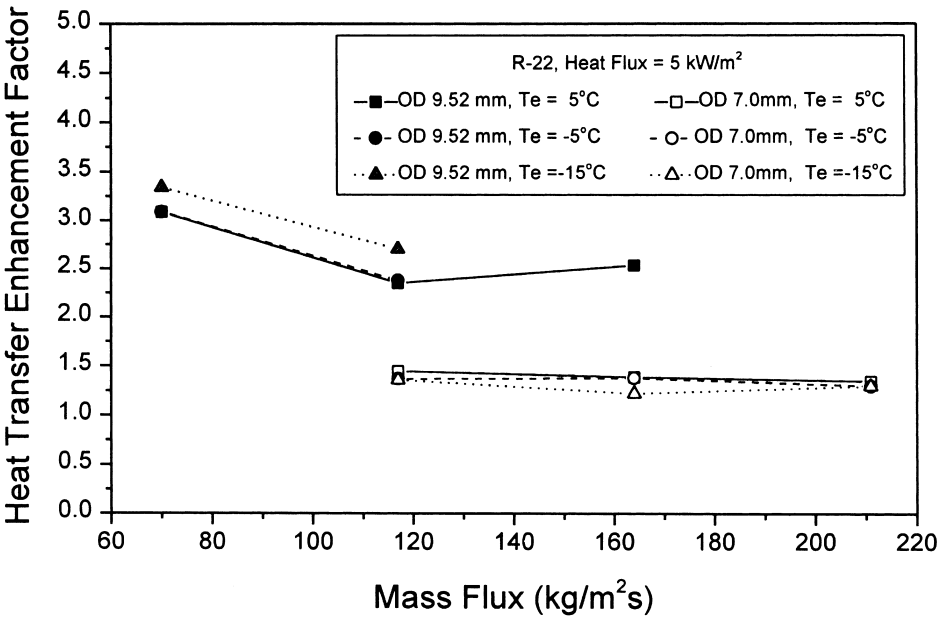

Fig. 13. Heat transfer enhancement factor with a heat flux of 5 kW/m^2.

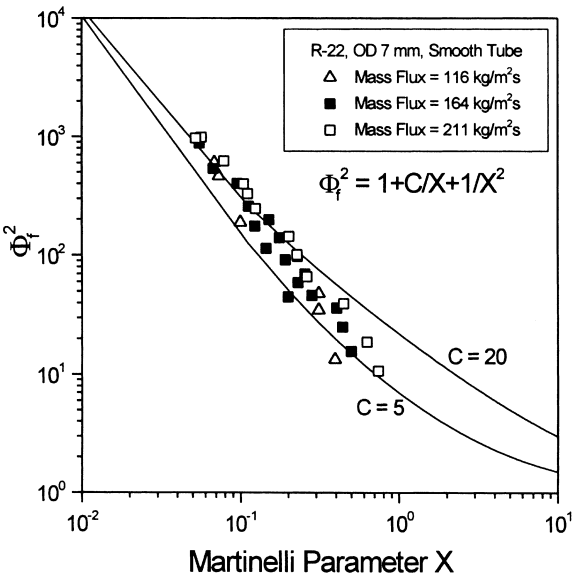

Fig. 14. Lockhart–Martinelli correlation vs. the experimental data.

to 164 kg/m^2 s. For the 7.0 mm OD tube, the EFs maintained fairly constant with respect to the mass flux. Eckels and Pate [10] reported the EF for the lower mass flux with the 9.52 mm OD tube was 2.5, while that for the higher mass flux was 1.5. It can be concluded from results of the present study that the micro-fin inside tube is more effective in the range of the lower mass flux and larger tube diameter.

4.4. Pressure drop

The two-phase friction multiplier, ϕ_f^2, for smooth, circular tube as proposed by Chisholm [12] can be represented as a function of the Martinelli parameter, X.

$$\phi_f^2 = 1 + \frac{C}{X} + \frac{1}{X^2} \tag{5}$$

where

$$X^2 = \frac{(dP_{F,f}/dl)}{(dP_{F,g}/dl)} \tag{6}$$

The constant C ranges from 5 to 20 depending on the Reynolds number of the liquid and vapor phase. If the both phases are in turbulent flow, the C is equal to 20. When the both phases are in the laminar flow, the C is 5. Fig. 14 shows the measured data plotted in the form of ϕ_f^2 vs. X and that predicted by the Eq. (5) for $C = 5$ and 20. Generally for the high quality region, the experimental data for the two-phase friction multiplier was larger than that predicted with $C = 20$. As the mass flux increased, the ϕ_f^2 became larger.

Fig. 15 shows the pressure drop per unit length for the smooth and micro-fin tubes at the specified mass flux (164 kg/m^2 s) and heat flux (5 kW/m^2). The inlet

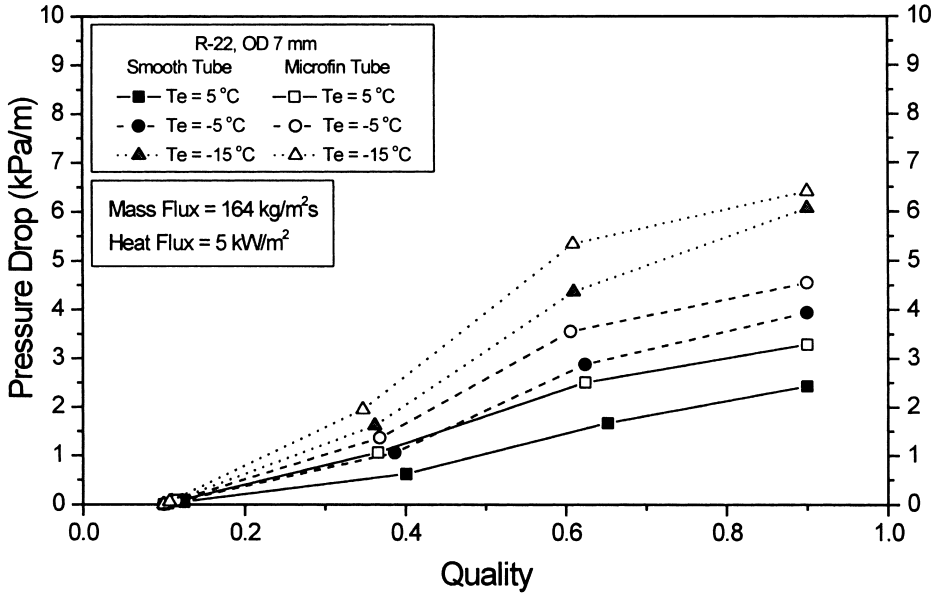

Fig. 15. Pressure drop with a mass flux of 164 kg/m^{2}s and a heat flux of 5 kW/m^2.

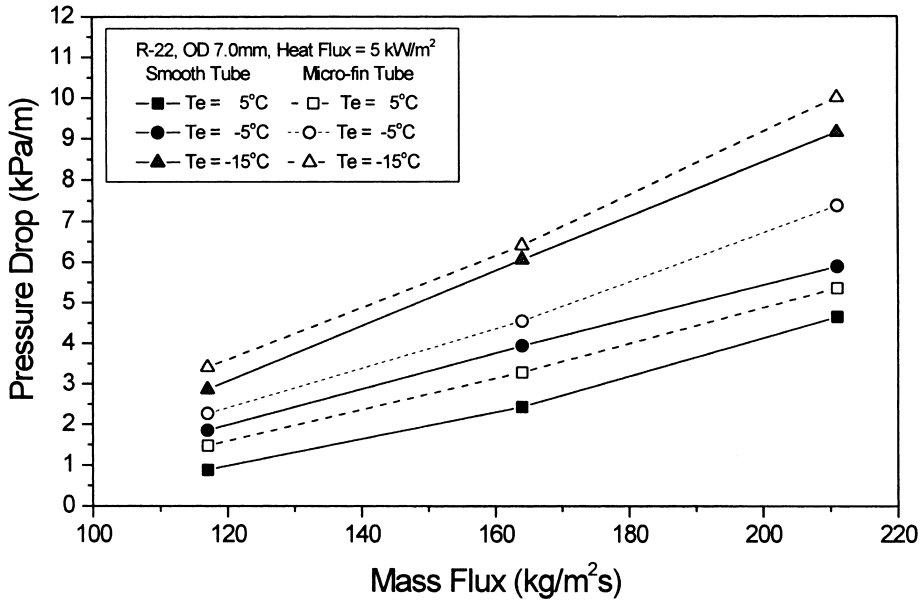

Fig. 16. Pressure drop with a variation of mass flux and evaporating temperature.

and outlet qualities were 10 and 90%, respectively. The pressure drop increased with quality. In addition, the pressure drop reduced significantly as the evaporating temperature increased. As the evaporating temperature increased, the drop of the liquid viscosity and the specific volume of the vaporized refrigerant leaded to the reduction of the refrigerant velocity and pressure drop. Fig. 16 shows the average pressure drop as a function of the mass flux at the specified heat flux (5 kW/m^2). For the given heat flux, the average pressure drop for both tubes was approximately proportional to $G^{2.36}$ at $T_e = 5°C$ and $G^{1.83}$ at $T_e = -15°C$. At lower evaporating temperature, the influence of mass flux on pressure drop was reduced. Kuo and Wang [2] showed

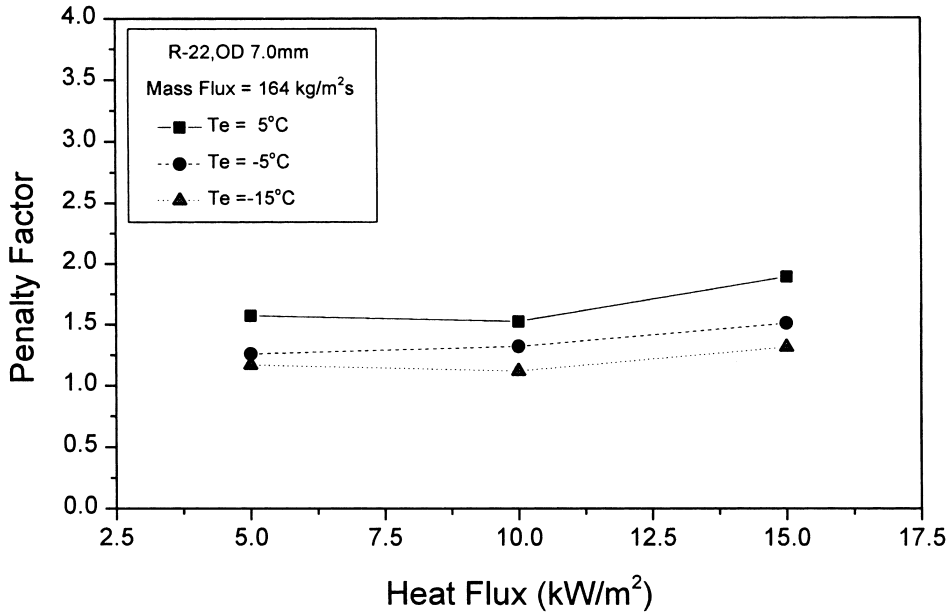

Fig. 17. Penalty factor with a mass flux of 164 kg/m^2 s.

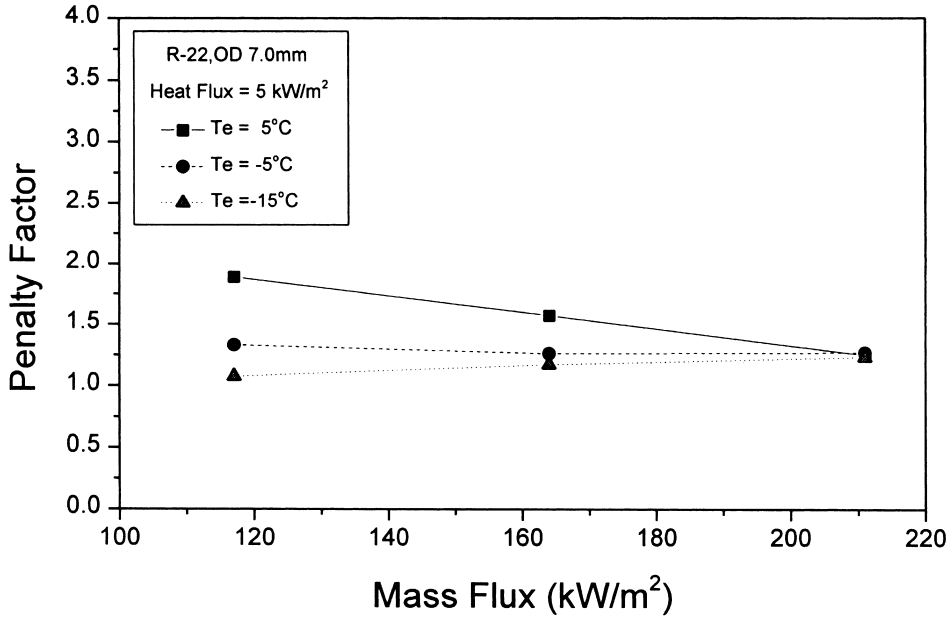

Fig. 18. Penalty factor with a heat flux of 5 kW/m^2.

that the pressure drop was proportional to $G^{1.65}$ (test condition: $T_e = 6°C$, $G = 100–300$ kg/m^2 s, $q'' =$ adiabatic condition and 9.52 mm OD tube). The effect of mass flux on the pressure drop for the micro-fin tubes was somewhat higher than that of the smooth tube.

Fig. 17 shows variation of the pressure drop penalty factor (PF) as a function of the heat flux at the mass flux of 164 kg/m^2 s for the 7.0 mm OD tubes. The PF was defined as the ratio of the pressure drop for a micro-fin tube to that for a comparable smooth tube at the similar flow conditions. Generally, the micro-fin tube showed more pressure drop than the smooth tube and the PF ranged from 1.1 to 1.9. The PF slightly increased with the heat flux. Fig. 18 shows variation of the PF as a function of the mass flux at the heat flux of 5 kW/m^2 for the 7.0 mm OD tubes. For lower evaporating temperatures, the PF had a relatively constant value of 1.2 with the mass flux, while for the evaporating temperature of 5°C, it decreased from 1.9 to 1.2 with the mass flux.

5. Conclusions

The experimental data on evaporation for the 9.52 mm and 7.0 mm OD micro-fin/smooth tube were presented. The experimental data were taken at the evaporating temperature of −15, −5 and 5°C, the refrigerant mass flux from 70 to 211 kg/m^2 s and the heat flux from 5 to 15 kW/m^2. The effects of heat flux, mass flux, evaporating temperature and tube diameter on the evaporation heat transfer coefficient were investigated.

For the micro-fin and smooth tubes tested in the present study, the evaporation heat transfer coefficient was enhanced with an increase of the mass flux and with a decrease of the evaporating temperature. The heat transfer coefficient for the smooth tube increased with an increase of the heat flux, while it for the micro-fin tube was slightly dropped. The enhancement of the heat transfer coefficient for the micro-fin tube over the smooth tube was significant in the 9.52 mm OD tube as compared to that for the 7.0 mm OD tube. The EFs for the 9.52 and 7.0 mm OD tubes tested in the present study were from 2.2 to 3.3 and from 1.2 to 1.8, respectively.

Pressure drop increased with the quality and mass flux. For the given heat flux, the average pressure drop for both tubes was approximately proportional to $G^{2.36}(T_e = 5°C) \sim G^{1.83}(T_e = -15°C)$. For lower evaporating temperatures, the PF showed relatively constant value of 1.2 with the mass flux. As the evaporating temperature decreased, the pressure drop per unit length increased. The PF slightly increased with the heat flux.

Acknowledgements

The authors wish to acknowledge the financial sup-

port of the Korea Research Foundation made in the program year of 1997.

References

[1] L.M. Schlager, M.B. Pate, A.E. Bergles, Evaporation and condensation heat transfer and pressure drop in Horizontal, 12.7 mm micro-fin tubes with refrigerant 22, J. Heat Transfer 112 (1990) 1041–1047.
[2] C.S. Kuo, C.C. Wang, In-tube evaporation of HCFC-22 in a 9.52 mm micro-fin/smooth tube, Int. J. Heat Mass Transfer 39 (1996) 2559–2569.
[3] C.S. Kuo, C.C. Wang, W.Y. Cheng, D.C. Lu, Evaporation of R-22 in a 7 mm micro-fin tube, ASHRAE Trans. 95 (1995) 1055–1061.
[4] S.J. Kline, F.A. McClintock, Describing uncertainties single sample experiments, Mech. Eng. 75 (1953) 3–8.
[5] V.E. Schrock, L.M. Grossman, Forced convection boiling in tubes, Nucl. Sci. Eng. 12 (1962) 474–481.
[6] S.G. Kandlikar, A general correlation for saturated two-phase flow boiling heat transfer inside horizontal and vertical tubes, J. Heat Transfer 112 (1990) 219–228.
[7] K.E. Gungor, R.H.S. Winterton, A general correlation for flow boiling in tubes and annuli, Int. J. Heat Mass Transfer 29 (1986) 351–358.
[8] J.C. Chen, Correlation for boiling heat transfer to saturated fluids in convective flow, I&EC Process Design and Development 5 (3) (1966) 322–329.
[9] R.M. Wright, G.F. Somerville, R.L. Sani, L.A. Bromley, Downflow boiling of water and *n*-butanol in uniformly heated tubes, Chem. Eng. Progr. Symp. Ser. 61 (1965) 220–229.
[10] S.J. Eckels, M.B. Pate, Evaporation and condensation of HFC-134a and CFC-12 in a smooth tube and a micro-fin tube, ASHRAE Trans. 97 (1992) 71–81.
[11] V.V. Klimenko, A generalized correlation for two-phase forced flow heat transfer, Int. J. Heat Mass Transfer 31 (1988) 541–552.
[12] D. Chisholm, A theoretical basis for the Lockhart–Martinelli correlation for two-phase flow, Int. J. Heat Mass Transfer 10 (1967) 1767–1778.